Analysis of Ice-to-Liquid Ratios during Freezing Rain and the Development of an Ice Accumulation Model

KRISTOPHER J. SANDERS AND BRIAN L. BARJENBRUCH

NOAA/National Weather Service, Topeka, Kansas

(Manuscript received 12 September 2015, in final form 17 March 2016)

ABSTRACT

Substantial freezing rain or drizzle occurs in about 24% of winter weather events in the continental United States. Proper preparation for these freezing rain events requires accurate forecasts of ice accumulation on various surfaces. The Automated Surface Observing System (ASOS) has become the primary surface weather observation system in the United States, and more than 650 ASOS sites have implemented an icing sensor as of March 2015. ASOS observations that included ice accumulation were examined from January 2013 through February 2015. The data chosen for this study consist of 60-min periods of continuous freezing rain with precipitation rates ≥ 0.5 mm h^{-1} (0.02 in. h^{-1}) and greater than a trace of ice accumulation, yielding a dataset of 1255 h of observations. Ice:liquid ratios (ILRs) were calculated for each 60-min period and analyzed with 60-min mean values of temperature, wet-bulb temperature, wind speed, and precipitation rate. The median ILR for elevated horizontal (radial) ice accumulation was 0.72:1 (0.28:1), with a 25th percentile of 0.50:1 (0.20:1) and a 75th percentile of 1.0:1 (0.40:1). Strong relationships were identified between ILR and precipitation rate, wind speed, and wet-bulb temperature. The results were used to develop a multivariable Freezing Rain Accumulation Model (FRAM) for use in predicting ice accumulation incorporating these commonly forecast variables as input. FRAM performed significantly better than other commonly used forecast methods when tested on 20 randomly chosen icing events, with a mean absolute error (MAE) of 1.17 mm (0.046 in.), and a bias of −0.03 mm (−0.001 in.).

1. Introduction and background

Branick (1997) found that notable freezing rain or freezing drizzle occurs in about 24% of all winter weather events across the continental United States. Proper preparation by utility, transportation, and public safety entities for these freezing rain events requires accurate forecasts of ice accumulation on various surfaces. As icing takes place during a freezing rain event, it ultimately results in two different types of ice accumulation that contribute to the majority of impacts: on roadways and sidewalks, and on tree branches and power lines. The impacts caused by reduced friction on roads and sidewalks are typically driven by the small amounts of ice accumulation that are required to coat the affected surface, while any additional icing results in similar impacts to that of the initial icing. In these cases, forecasting the initial ice accumulation sufficient to coat the surface may be the most important part of the forecast. Predicting ice accretion on the roadways and sidewalks depends on many factors such as surface, air, and soil temperatures; insolation; an elevated or nonelevated surface; exposure to wind; amount of traffic; and the presence of treatment chemicals. Reduced-friction impacts as well as ice accumulating on tree branches and power lines are of great importance to public safety. It is the ice accumulation on these elevated surfaces that can cause significant damage to property and infrastructure across a widespread region. These impacts are a direct result of the magnitude of the ice accumulation, and damage can quickly occur after structural stress thresholds are exceeded. The effects of ice on electrical transmission and distribution lines can cause power outages that last several weeks in some areas, according to Changnon and Creech (2003). Accurate forecasts for ice accumulation magnitude are of the utmost importance in predicting and appropriately planning for these potentially catastrophic ice storm impacts. A record of standardized and accurate ice

Corresponding author address: Kristopher J. Sanders, NOAA/NWS/Weather Forecast Office, 1116 NE Strait Ave., Topeka, KS 66616.
E-mail: kris.sanders@noaa.gov

DOI: 10.1175/WAF-D-15-0118.1

thickness measurements is also important to accurately describe the outcome of these events.

Ice accretions have been classified according to source and outward appearance (Makkonen 1984). Glaze and rime ice, which occur in many freezing rain events, form out of supercooled water droplets. Glaze is a hard, nearly bubble-free and clear homogeneous ice with a density close to 0.92 g cm^{-3}, the density of pure bubble-free ice. Glaze ice grows "wet," and liquid may pool or run along or off the surface. Rime ice, on the other hand, grows "dry," that is, water droplets impinging on the structure freeze on impact. Hard rime is a rather hard, granular, white or translucent ice with a density between 0.6 and 0.9 g cm^{-3}. Soft rime is white ice with a loose structure and a density less than 0.6 g cm^{-3}. The density of pure liquid water is 1.0 g cm^{-3} at a temperature of 0°C, therefore, making it denser than ice. Ackley and Templeton (1979) identified variables necessary to quantify the amount and character of accreted ice on a surface: 1) ambient air temperature, 2) cloud liquid water content and droplet size distribution, 3) wind speed, and 4) cross-sectional area and shape of the object. When an object or surface is exposed to icing conditions, the rate of ice accretion is governed by two processes that depend on the above variables: the impingement of supercooled water droplets on the surface and the thermodynamics at the surface, which determines what portion of the impinging liquid freezes, runs off the surface, and melts previously accreted ice. Ice accretion efficiency is also dependent upon the material on which accretion is occurring, the temperature of that object, orientation relative to the wind, and color and albedo effects.

In essence, heat must be removed from the impinging water to allow it to freeze, and as ice develops, heat must continue to be removed from the ice surface. Adding heat to the water and ice surface takes place through 1) shortwave solar radiation during the daytime, 2) release of heat during fusion of water, 3) sensible heat transfer between accreting drops and the surface, 4) viscous heating from airflow around the object, 5) kinetic energy transferred from the falling drops to the ice, and 6) longwave radiation from the ground surface below. Removing heat from the water and ice surface takes place through 1) loss of heat due to wind near the surface or free convection in the absence of wind, 2) cooling due to evaporation of the impinging water that does not immediately freeze to the surface, and 3) longwave radiative cooling emitted from the ice surface. The aforementioned ice accretion methods that make up this process (e.g., cloud liquid water content, droplet size distribution, solar radiation, latent heat, kinetic energy, evaporational cooling) are not typically forecasted by the meteorological community, rendering some ice accretion models difficult to use in an operational environment.

Freezing rain accretion is substantially regulated by the total mass flux, the vector sum of the vertical and horizontal mass fluxes, as it contributes to the amount of water collected on a surface. Vertical mass flux is well approximated by the precipitation rate, but can be more definitively computed by the amount of water falling vertically at terminal velocity in the absence of wind. Horizontal mass flux is influenced by wind velocity and the drop size distribution or liquid water content. The magnitude of the horizontal mass flux onto a surface will vary based on the orientation of the object relative to the wind vector, which will be maximized when an object is perpendicular to the wind. (i.e., a power line that is orientated perpendicular to the wind has more surface area for the horizontal mass flux than if the power line was parallel to the wind. The same is true for tree branches, but their orientation can vary greatly within the tree). A robust examination of freezing rain processes by Jones (1996, hereafter J96), of the Cold Regions Research and Engineering Laboratory (CRREL), showed that ice accretion is highly dependent upon the wind speed, which contributes to removing heat from the ice surface while also increasing the horizontal mass flux of the falling precipitation. Additionally, water that does not immediately freeze to an elevated surface can freeze during the process of running off to form icicles. Icicles do not contribute to the ice accretion thickness, making this thickness difficult to predict, but they do contribute to the mass of the ice, which the object will have to support. J96 explains that icicles are more likely to form in conditions with near-freezing temperatures and light wind speeds versus colder or windier scenarios.

Over the past 50 years there have been several attempts to model ice accretion, most in the interest of governing wind-on-ice loads (i.e., engineering designs) for electric power transmission lines and communication towers. The Chaîné model (Chaîné and Castonguay 1974) was developed based on wind tunnel tests to investigate sea spray icing. While effective in its initial intent, this model made a number of assumptions and extrapolations in order to convert sea spray icing data into a formulation for freezing rain. Makkonen (1998) investigated the modeling of power line icing in freezing precipitation. The work of J96 also led to the development of a pair of ice accretion models. One of these models developed by Jones was a complete heat-balance model, hereafter referred to as the CRREL HBM, while the second was a simple flux model (Jones 1998, hereafter J98), hereafter referred to as the CRREL SM. More recently, DeGaetano et al. (2008) developed an

ice accumulation method using forecasted precipitation amount, wind speed, and the thermodynamic profile of the lower atmosphere from the Weather Research and Forecasting Model in combination with the ice accretion model described by J98 and a modified precipitation-type algorithm. Musilek et al. (2010) described an ice accretion forecasting system based on a numerical weather prediction (NWP) model combined with a precipitation-type classifier and ice accretion model.

In a joint effort between the American Society of Civil Engineers (ASCE), CRREL, the National Climatic Data Center [NCDC; now known as the National Centers for Environmental Information (NCEI)], the Air Force Combat Climatology Center, the National Weather Service (NWS), and the Federal Aviation Administration, a climatology of extreme ice thicknesses from freezing rain and concurrent wind speeds was developed for a 50-yr return period for the eastern half of the country (ASCE 2002). This information is utilized for national electric safety codes, guidelines for electric transmission line structural loading, and structural standards for steel antenna towers and supporting structures. Ultimately, the CRREL HBM and CRREL SM developed by J96 and J98 were used to replicate past ice storms in combination with the peaks-over-threshold method with the generalized Pareto distribution (Hosking and Wallis 1987) to develop the wind-on-ice loads for a 50-yr return period. The CRREL SM was developed for use with data inputs commonly measured in real time via existing instrumentation, presumably giving it value as a forecast tool, while the CRREL HBM requires input variables not commonly measured in real time or forecast in operations. All of the past studies involved extensive computer modeling, laboratory, and field tests, and describe in great detail the complexity of ice accretion. One thing lacking from some of these findings is how this information can be utilized in an operational forecasting setting. Of course, NWP model-derived ice accumulation can be useful for ice forecasting, but these values rely heavily on model output, biases, and precipitation-type algorithms.

The ice:liquid ratio (ILR) is the ratio of the accumulated ice depth on a particular surface to the accumulated liquid depth that, by definition, is on a horizontal surface. Investigation into ILR could reveal ice accretion efficiencies and the effects of these aforementioned commonly measured weather variables. Recall that the bulk densities of both liquid water and ice suggest that theoretically this ILR on horizontal surfaces should be close to 1.09:1 at 0°C, but can be highly variable because of the many complexities. Given a minimal amount of research dedicated toward the operational prediction of ice accretion efficiency, some commonly used operational forecaster techniques include a simple 1.0:1 ILR, raw output from NWP models, or use of a more arbitrary ILR to produce ice accumulation forecasts. The authors have also noted that some operational forecasters have adopted the CRREL SM to compute ice accumulation forecasts based on the use of commonly forecast weather variables; therefore, it has been chosen for further analysis within this study.

It is imperative that ice accumulation predictions all implement descriptors of the type of ice thickness being addressed, as any preparations to be made will depend substantially on the details of the predicted ice thickness and associated impacts. Furthermore, ILR changes meaning depending upon how the ice accumulation is measured. There are four unique ice thickness measurements related to freezing rain and drizzle, as shown in Fig. 1, which will be referred to during this study. These include ice thickness on an elevated horizontal surface T_i, equivalent radial ice thickness on an elevated surface R_{eq}, equivalent diameter ice thickness on an elevated surface D_{eq}, and ice thickness on a horizontal ground surface G_i. These measurements have, to some extent, been used interchangeably and without specificity in the operational realm, including ice storm reports contained in numerous data archives. Variations in the shape of the ice accumulation also occur as a result of wind speed and direction, precipitation rate, freezing rate, wet versus dry growth, and icicle development. Ice accreting on tree branches and power lines can form a nonuniform depth around the object, giving one side a greater thickness, as seen in Fig. 2a. Under certain conditions, icicles can form on the bottom or side of an object, and occasionally the ice thickness is negligible compared to the amount of icicles, as shown in Fig. 2b. As a result of varying geometry, flux exposure (i.e., sensible heat from the ground), and ice growth (i.e., wet and dry ice growth), the ice accretion efficiency for various types of icing and associated ILRs can be quite different and in some cases not directly comparable. Within this work, T_i and R_{eq} are used exclusively in defining ILR, which can be directly related to the ice mass.

A majority of the ice accretion model verification studies do not provide any information regarding ILRs, which are very applicable to operational forecasting. There has been no attempt to collect an extensive ice thickness measurement dataset, similar to the one deployed during the Automated Surface Observing System (ASOS) ice sensor project (covered in more detail in section 2), for utilization in a forecast verification study. This has resulted in a lack of applicable and detailed information available to the meteorological community regarding ILRs. More specifically, the knowledge base of the operational forecasting community is lacking regarding the physical processes of ice accretion and how they directly affect these ILRs.

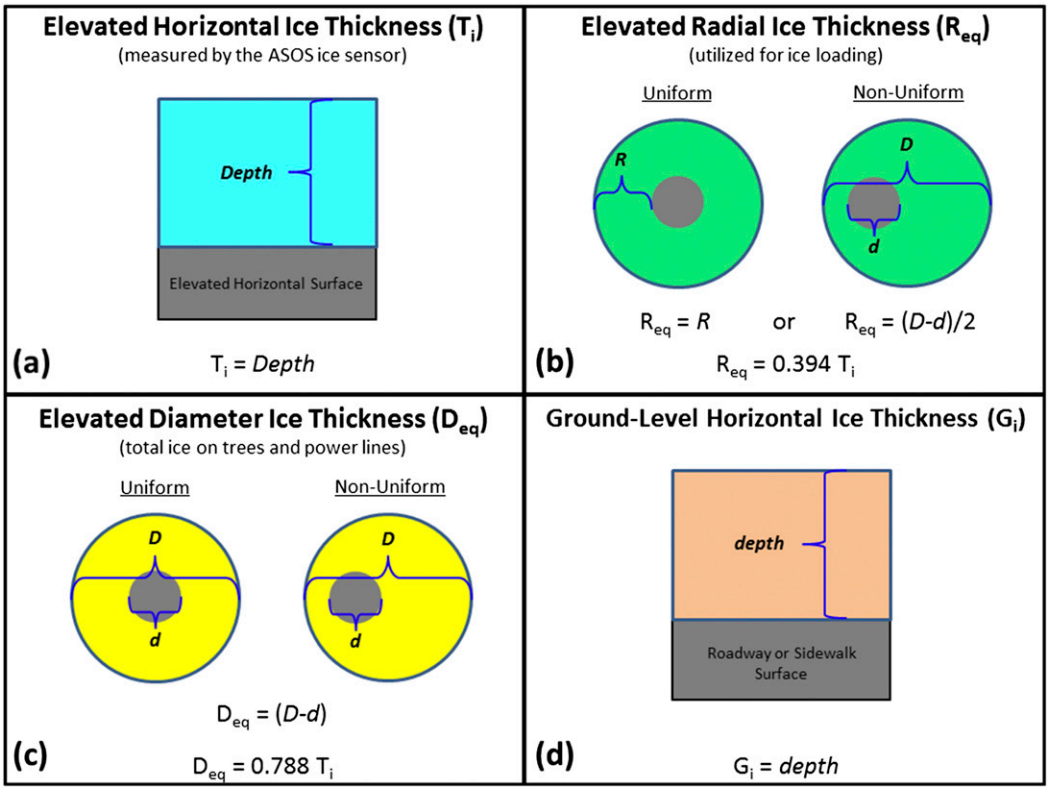

FIG. 1. Visual representation of commonly used ice thickness measurements. (a) Elevated (1.5 m) horizontal ice thickness for vehicle surfaces and grounded airplane wings, (b) elevated radial ice accumulation for power lines and tree branches, (c) elevated diameter ice accumulation or total ice accumulated on power lines and tree branches, and (d) ground-level horizontal ice accumulation for roadway and sidewalk surfaces. Conversions shown here between R_{eq}, T_i, and D_{eq} were derived in RR07.

The focus of this study is on investigating how ILRs change in varying environmental conditions using a large, geographically diverse, and objectively observed set of ASOS data. These data are analyzed to identify any relationships between ILR and various meteorological observations including precipitation rate, wind speed, temperature, and moisture. This information will be used to develop improved forecast methods and provide comparison to existing commonly used ice accretion forecast models. More importantly, the analysis from the data collected could be used to increase the knowledge of ice accretion efficiency and, ultimately, improve the ice accumulation forecast process within the NWS and the meteorological community as a whole.

2. Data and methodology

a. ASOS ice measurements

The first step in better understanding and forecasting ice accretion is to obtain a robust, diverse, and objective dataset of ice thickness measurements during freezing rain events, collocated with observations of other meteorological variables. Unfortunately, recent ice accretion model verification studies have only utilized manually collected observations from a relatively small number of freezing rain events. The authors have found that NCDC *Storm Data* does contain a large number of ice measurements from past events, but the measurements can be subjective and often do not specify the type of measurement taken (T_i, R_{eq}, D_{eq}, or G_i). *Storm Data* is often vague regarding ice shape or measurement surface, and at times only includes a brief description of measurements over a large geographic area (e.g., one entire county), making it difficult to determine actual amounts of both ice and liquid at a specific location as well as the time frame during which ice accumulated. All of these factors contribute to the subjective nature of the *Storm Data* measurements, with plenty of uncertainty and potential for inaccuracy; therefore, this dataset has not been included in the observational database for this work.

Technological advancements have recently provided an opportunity to measure real-time ice accretion in

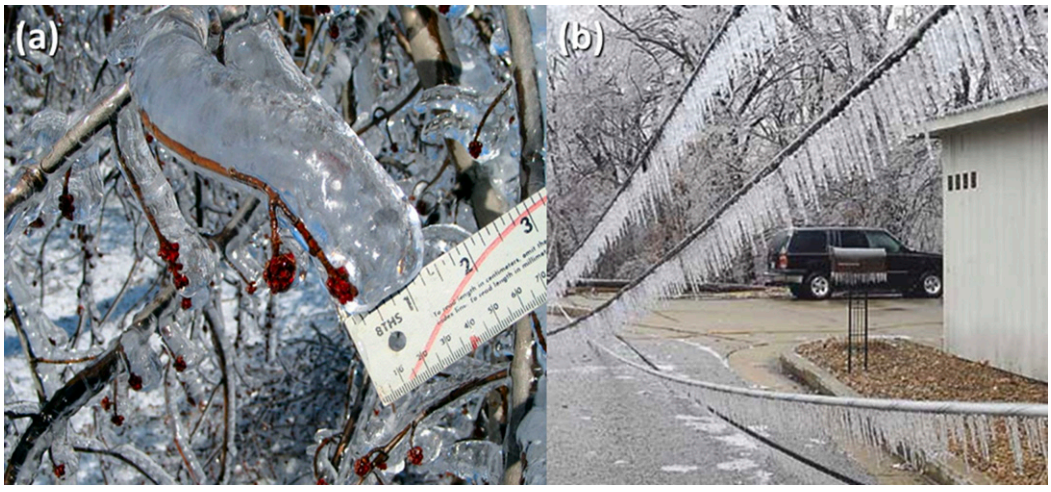

FIG. 2. (a) Ice-covered trees near Kearney, NE, 29 Dec 2006. (Photograph courtesy of the NWS Weather Forecast Office in Hastings, NE.) (b) Ice accumulation on power lines and trees in Jefferson City, MO, on 8 Dec 2007. (Photograph courtesy of the NWS Weather Forecast Office in St. Louis, MO.)

combination with meteorological conditions during freezing rain events. The ASOS has become the primary surface weather observation system in the United States with more than 880 sites commissioned. As of March 2015, at least 650 ASOS sites were equipped with the Goodrich Sensor System (formerly Rosemount) 872C3 icing sensor (Fig. 3), providing ASOS the ability to report freezing rain in real time (Ramsay and Laster 1995). The icing sensor detects ice by sensing ice mass on a 25-mm-long by 6-mm-diameter vertical probe that vibrates longitudinally at a nominal 40 kHz when ice free. Ice mass on the sensor is determined by monitoring the minute-to-minute frequency of the icing sensor and multiplying the net frequency change (NFC) or decrease (from 40 kHz) by a manufacturer-specified ice-thickness factor (NWS 1995). An algorithm based on raw data from the icing sensor has demonstrated reliable quantitative estimates of ice accretion (Ryerson and Ramsay 2007, hereafter RR07). The goal of RR07 was to compare and calibrate the ASOS ice sensor during the winters of 1995–2002 and in doing so they demonstrated the capabilities of the sensor.

RR07 focused on collecting and comparing ice sensor measurements to manual measurements of ice thickness as well as mass on a standard surface in proximity to ASOS test sites. For comparison and calibration purposes, ice mass was manually monitored on aluminum cylinders suspended horizontally at 1.5 m above ground level, and a separate horizontal aluminum plate at the same height was also used to take measurements of ice mass and ice thickness T_i. Figure 4 from RR07 shows the actual ice mass measurements for one particular icing event (14–15 January 1999) during the study, as well as the ice mass approximated by each ice sensor deployed throughout the entirety of the event. The study ultimately identified a direct relationship between the sensor frequency changes and ice accretion magnitude when comparing ASOS-reported ice depths with the measurements taken during the field study. During the

FIG. 3. Goodrich Sensor Systems (Rosemount) Model 872C3 icing sensor used at all ASOS stations equipped with ice detectors.

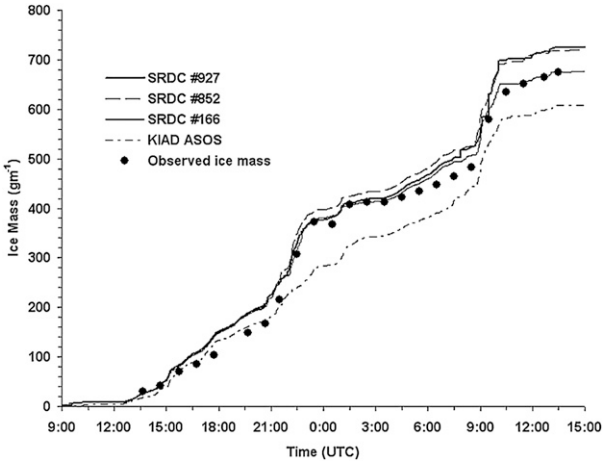

FIG. 4. The 14–15 Jan 1999 icing event at the NWS Sterling, VA, Research and Development Center (SRDC) showing measured ice mass increase during the storm, as well as ice mass increases predicted from each of the four ice detectors. Note that the best matches are among the ice detectors that are collocated at SRDC. Correlations between the measured ice mass and the predicted masses were all greater than $r = 0.98$, with standard errors of less than 37.3. (This figure was taken from RR07.)

observational period of four winter seasons, data were obtained during approximately 188 h of icing conditions. The final analysis revealed there was a correlation coefficient of 0.98 between the cumulative cylinder ice mass and NFC detected by the ice sensor through the entire study Fig. 5a. Ice thickness factors used for conversions were found for each possible measurement. Ultimately, ice thickness on an elevated horizontal surface (T_i) was chosen as the final output of this sensor. Using each measurement of ice mass concurrent with NFC during the field study, RR07 derived the R_{eq} to be compared to the corresponding ice thickness of T_i. Figure 5b from RR07 shows the relationship between R_{eq} and T_i for the 537 data pairs with a linear expression:

$$R_{eq} = 0.394 T_i. \quad (1)$$

Therefore, ice depth T_i may be used to infer ice accretion on elevated cylindrical objects in terms of R_{eq}. This relationship essentially bridges the gap between the two types of ice measurements and can be used to convert ASOS ice accumulations to equivalent radial accumulations. This is a slightly different conversion compared to the relationship between G_i and R_{eq}, which is a factor of $1/\pi$ through simple geometry, since T_i is an elevated surface and susceptible to runoff.

There are five limitations of the ASOS ice sensor and algorithm described in detail by RR07. Limitations of greatest importance to this work include the following. 1) Goodrich Sensor Systems were delivered if they passed a manufacturer's "rate test," in which a sensor's response to a specific ice amount and icing rate was required to be within 20% of a nominal value. 2) Ice accretion below the reporting frequency threshold was identified (i.e., a minimum frequency decrease of 33 Hz, with a concurrent rate of decrease of at least 13 Hz in 15 min), which provides a "cushion" to ensure that the system will not issue a false alarm of freezing rain. This only accounted for 6% of all RR07 recorded icing. 3) The ASOS reporting algorithm for freezing rain extends the weather type of freezing rain "FZRA" within the aviation routine weather report (METAR) for an additional 15 min after the ice sensor no longer detects accretion. This accounts for intermittent showers and eliminates the need for multiple special reports. 4) Clamping, or the increase in frequency caused by ice

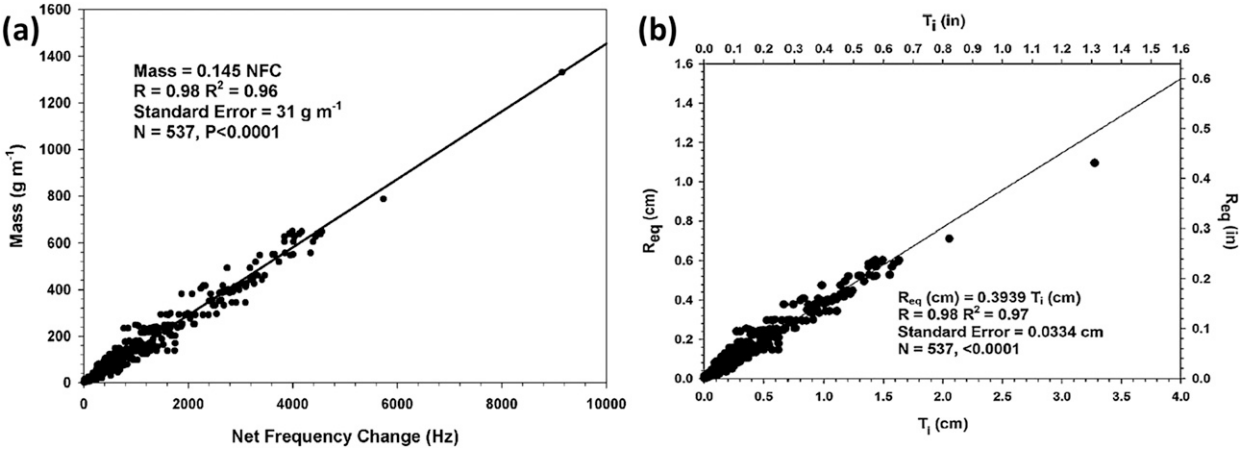

FIG. 5. (a) Relationship between NFC (Hz) and ice mass accumulated on ice-rack horizontal aluminum rods. (b) Linear relationship between equivalent uniform radial ice thickness R_{eq} and horizontal planar ice thickness T_i. (These figures were taken from RR07.)

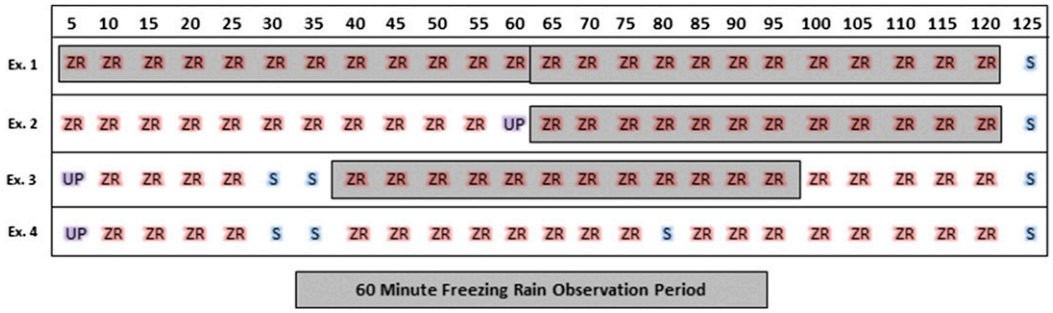

FIG. 6. The 60-min freezing rain observation period selection criteria. In these examples, abbreviations are identical to those used in METAR code (ZR, freezing rain; UP, unknown precipitation type, and S, snow). Example 1 illustrates how two 60-min observation periods are extracted from 120 min of continuous freezing rain. Examples 2–4 illustrate various situations for which nonfreezing rain precipitation is introduced within the 5-min observations.

bridging at the base of the probe, affects estimates of ice accretion, which only accounted for 4% of all RR07 recorded icing. 5) A slow deicing cycle recovery time when the sensor may fail to report ice accretion for up to 30–45 min, which only accounted for 2% of all RR07 recorded icing. RR07 ultimately provided incentives not to change the ASOS ice-thickness factor given the less than 20% sensor variability allowance due to manufacturing specifications. This variability allowance was also uniformly allowed to be ±20%, resulting in no appreciable bias when utilizing a number of sensors. Limitations of the ice accretion algorithm were thoroughly examined by the NWS and were deemed acceptable, resulting in a formal directive to proceed with the ice sensor implementation (NWS 2000). ASOS software version 3.07 was released in November 2012, featuring the dissemination of ice accumulation observations within the remarks section of the METAR reports. This was followed up with the release of ASOS software version 3.10 in May 2013, which provided this capability to a greater number of ASOS sites. Given these results were being disseminated and deemed acceptable, an analysis of ASOS icing data, in conjunction with standard weather observations, could allow an in-depth examination of ILR.

b. *ASOS ice data and processing*

The 5-min observations from every ASOS with a Goodrich icing sensor were obtained from NCDC for the period from January 2013 through March 2014 and also from October 2014 through February 2015. Data were gathered for all of these ASOS sites regardless of location, resulting in a geographically diverse dataset. This set of observations was reduced to only those 5-min observations that contained an ice measurement or freezing precipitation, a total of 81 256 observations. It was determined that 5 min was too short a duration to identify meaningful ILR due to trivial ice accumulations. To reconcile this limitation, 60-min periods of continuous freezing rain with no mixed precipitation were identified, resulting in 2445 observation periods. For comparison, utilizing 30-min periods would have resulted in a 27% increase in the total time of ice accretion in the dataset, but would have also resulted in a much less diverse population of ILR (e.g., a far greater count of round 1:1 or 2:1 ILR), similar to what occurs with 5-min observations. Another reason the 60-min periods were chosen was that current operational forecasts are created in hourly increments, and certain NWP models compute output in hourly increments as well.

The 60-min periods were allowed to begin at any 5-min observation time as long as they satisfied the criteria of nonmixed freezing precipitation (FZ) reported in consecutive 5-min observations for 60 min (Fig. 6). Using 5-min observations provides higher temporal resolution than a singular hourly ASOS observation in identifying persistent pure freezing rain events, and also provides greater temporal detail in other meteorological data measured by ASOS over the course of the full hour. Liquid precipitation and ice accumulation were summed over the 60-min period, while nonprecipitation observations (temperature, wind speed, wet-bulb temperature, etc.) were recorded as the mean in order to represent the entirety of the 60-min period.

The intent of this work was to examine freezing rain events that have the potential to cause notable infrastructure interruptions, so any 60-min periods with precipitation rates $< 0.50\,\mathrm{mm\,h^{-1}}$ ($0.02\,\mathrm{in.\,h^{-1}}$) were removed from the dataset. Any 60-min periods with trace amounts of ice accretion were also removed as a trace did not offer a reliable measurement for which to calculate the ILR. Finally, every 60-min period of observations underwent a manual quality control process to remove any periods during which the sensor failed to

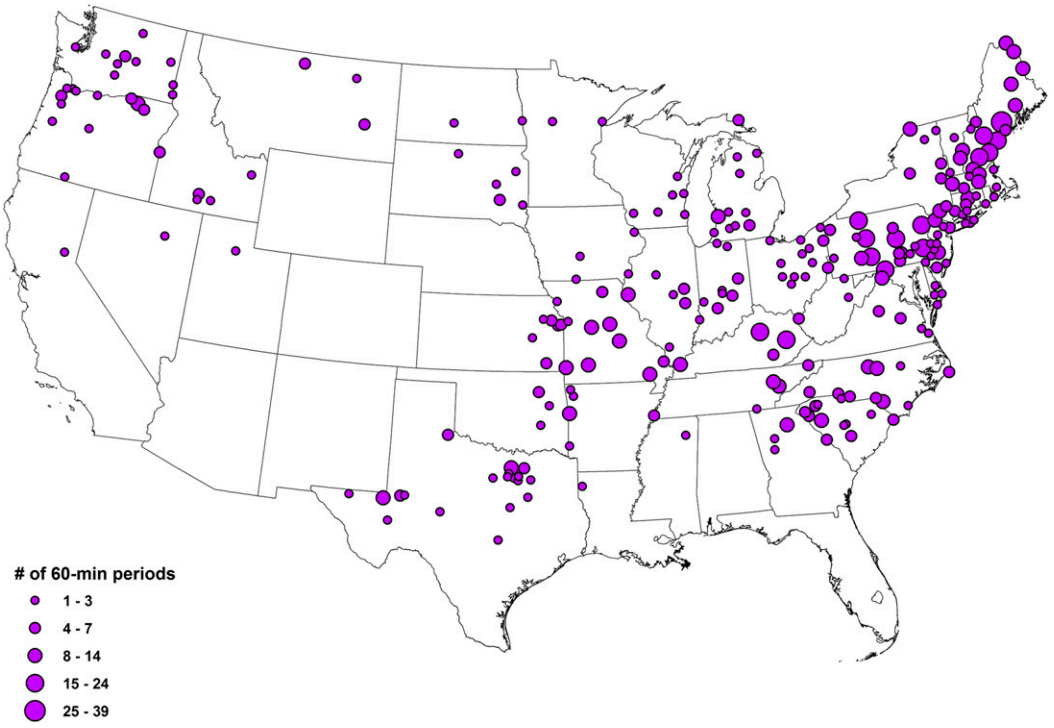

FIG. 7. ASOS icing locations from the final dataset, and the number of 60-min freezing rain observations per site.

record any of the meteorological data required to calculate the mean sustained wind speed or wet-bulb temperature data, or if the recorded data were not meteorologically reasonable (e.g., >10:1 ILR during a freezing rain event). The final dataset consisted of 1255 quality-controlled, 60-min periods of consecutive 5-min ASOS freezing rain observations for which the precipitation rate was $\geq 0.50\,\text{mm}\,\text{h}^{-1}$ ($0.02\,\text{in.}\,\text{h}^{-1}$) and the ice accumulation rate was $\geq 0.25\,\text{mm}\,\text{h}^{-1}$ ($0.01\,\text{in.}\,\text{h}^{-1}$). ASOS icing locations from the final dataset and the number of 60-min freezing rain observations per site are displayed in Fig. 7.

The 1255 h of freezing rain data were further separated during the development of the predictive model addressed in section 4. An analysis dataset was used to develop the predictive model, while a subset of data was held separate to be used as a nonbiased control dataset for objective analysis of predictive skill. This control dataset consisted of 20 freezing rain events, randomly selected at equal intervals across the unsorted dataset. The control dataset is composed of ''events'' as the operational meteorology community is typically focused on the freezing rain accumulation over the course of a weather event, while it provided analysis of the cumulative error of predictive methods rather than that of individual hours. An event was defined as the set of freezing rain observations during a continuous precipitation event at a single ASOS site satisfying the following criteria: 1) contained a period of ≥3 h of continuous freezing rain, 2) any events occurring on the same date must be ≥300 km apart, 3) there were no temporal gaps of ASOS-recorded precipitation >1 h within the event, and 4) there were no temporal gaps in ASOS-recorded freezing rain >12 h. The final analysis dataset consisted of 1161 h of freezing rain while the control group of freezing rain events included 94 h of freezing rain.

3. Results

ILRs were calculated for elevated horizontal ice accumulations, while the radial and diameter ILRs were derived based on the relationship from RR07 in Eq. (1). Given that these thicknesses contribute to different impacts, all of the values expressed in this section are in terms of T_i (R_{eq}). Of the 1255 total hours of freezing rain analyzed, a majority of the ILRs were between 0.50:1 (0.20:1) and 1.0:1 (0.40:1), which were the 25th and 75th percentiles, respectively, as seen in Fig. 8. The median value is 0.72:1 (0.28:1), while the mean value is slightly higher at 0.87:1 (0.34:1). Recall that the density of ice is approximately 8.3% less than liquid water, and that a simple physical relationship would suggest the mean ILR would be near 1.09:1 for horizontal surfaces. Considering the complexities of freezing rain accumulation,

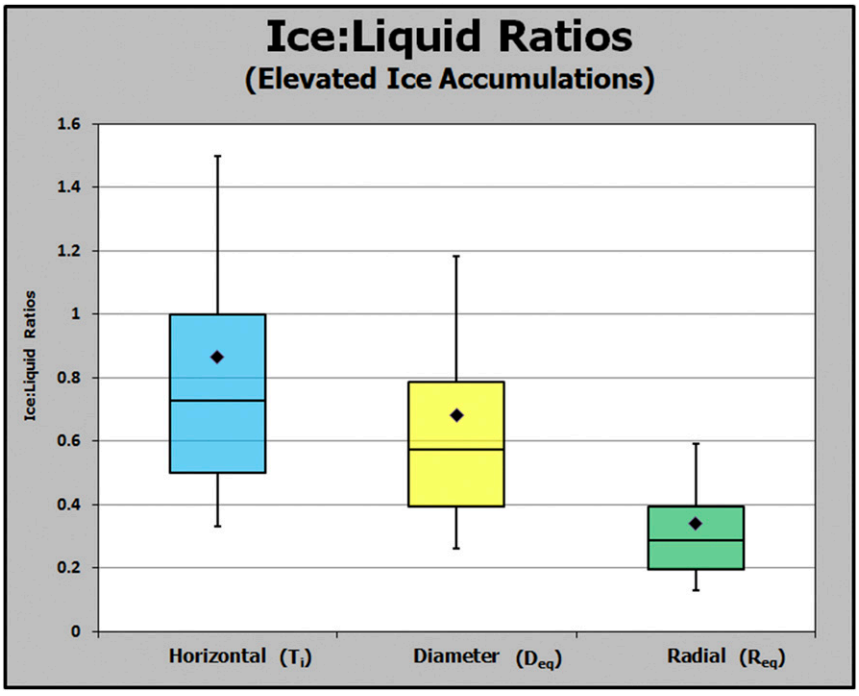

FIG. 8. Box-and-whisker plot of all ILRs. The shaded box encompasses the 25th–75th percentiles for elevated horizontal T_i (blue), diameter D_{eq} (yellow), and radial R_{eq} (green) ice accumulations; the whiskers extend to the 10th and 90th percentiles with the median (horizontal line) and mean (diamond) indicated.

this theoretical density-based ratio could be altered. It is possible, depending on the wind speed and particle size distribution, for the wind-driven component of the liquid flux to be substantially greater than the precipitation component. Conditions with smaller particles and higher wind speeds can cause considerably more ice on an elevated object than may be detected on the ground (or in a precipitation gauge). Also, the formation of both glaze and rime ice is possible, which have varying densities that ultimately contribute to varying ice thickness. The data clearly illustrate that these factors are important and imply that physical processes and atmospheric conditions influence icing efficiency, typically toward decreased efficiency. RR07 documented that ice thickness on the elevated horizontal plate in some cases would form an uneven surface, becoming more susceptible to runoff. Furthermore, using a standard 1.0:1 ILR in a forecast situation would typically lead to an overestimation of ice accumulations based on these results. It was found that ratios above 1.50:1 (0.60:1) and below 0.30:1 (0.12:1) were the least frequent. Figure 8 shows there was no interquartile overlap between the 75th percentile of the radial ILR and the 25th percentile of the horizontal ILR, illustrating the substantial difference between the two types of thicknesses.

Numerous previously discussed factors influence ice accretion and ultimately determine ILR. Some of these elements, such as heat and mass fluxes, are not typically forecasted by the meteorological community, nor easily measured with an abundance of commissioned sensors. This study will only focus on the commonly forecast weather elements measured by ASOS (e.g., precipitation rate, wind speed, temperature, and dewpoint), given the goal of improving the prediction process. Each weather element was examined independently to identify any contribution to the ILR, as well as any data trends.

a. Diurnal cycle

Investigation of the freezing rain observations revealed a strong association between the time of day and the frequency of freezing rain occurrence. Figure 9 shows an obvious minimum in freezing rain occurrence during the early afternoon, with a steady increase through the evening, and a peak in occurrence during the early morning. This may be due to a variety of factors, including the diurnal flux of shortwave solar radiation and surface temperatures that trend toward a minimum during the overnight, creating an environment more conducive to freezing rain and ice accumulation.

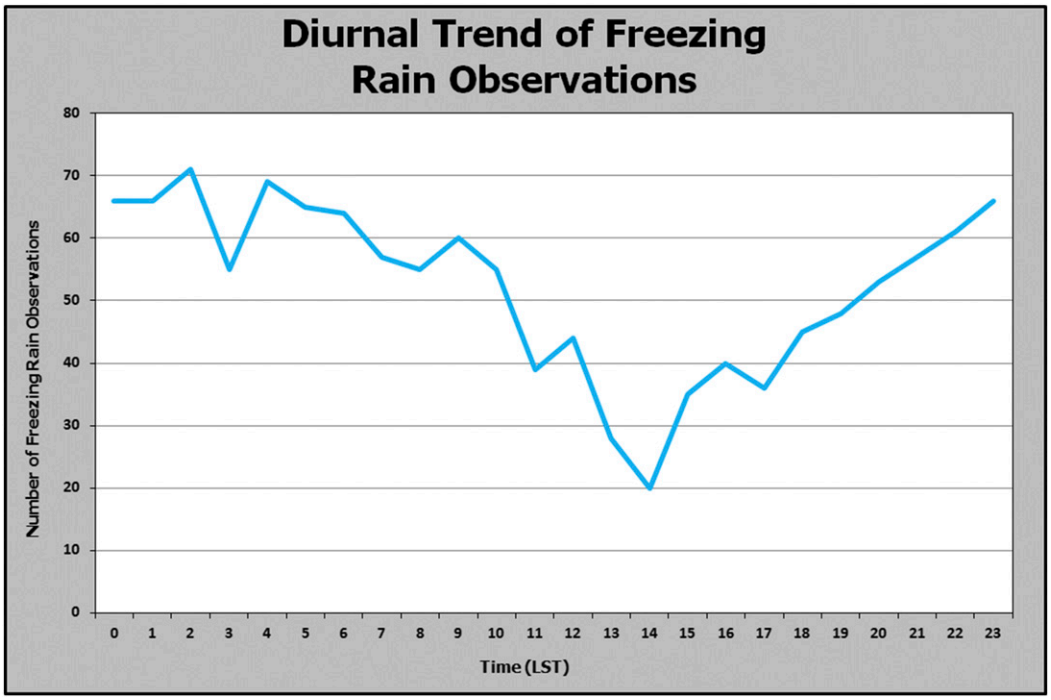

FIG. 9. The number of freezing rain observations per hour (LST).

b. Precipitation rate

Precipitation rate is important for ice accretion and ice accretion rates. Unfortunately, related variables such as drop size distribution and liquid water content, which also impact ice accretion, are not easily measured in the field, making them difficult to analyze. Recall that this methodology involved the removal of any 60-min observation with a precipitation rate $< 0.5\,\mathrm{mm\,h^{-1}}$ ($0.02\,\mathrm{in.\,h^{-1}}$) in an effort to eliminate the majority of freezing drizzle, as well as the typically low-impact, very-light-precipitation events. Out of the 1255 total hours of observed freezing rain, precipitation rates tended to be relatively light, with 1051 h containing $<2.54\,\mathrm{mm\,h^{-1}}$ ($0.10\,\mathrm{in.\,h^{-1}}$). This supports previous work by Sanders et al. (2013), who found that major ice storms in the central United States were relatively light precipitation events that persisted over long durations, eventually leading to substantial ice accumulations.

The observed precipitation rate data have a negative relation to ILR, as seen in Fig. 10. In fact, the highest ILRs tend to occur almost exclusively with the lighter precipitation rates [$<1.3\,\mathrm{mm\,h^{-1}}$ ($0.05\,\mathrm{in.\,h^{-1}}$)]. Examining the trend of the median value shows that ILR decreases exponentially, approaching a lower bound as the rates increase. Variability in the ILR also decreases as the precipitation rate increases, which is most easily visualized by the decreasing interquartile spread with increasing precipitation rate. It is implied that the lower ILRs with higher precipitation rates are due to a greater likelihood of runoff as the liquid may not have time to freeze before additional liquid is added to the ice surface. It is also possible that sensible heat added from excess liquid water on the ice surface affects the icing efficiency as well.

c. Sustained wind speed

An examination of all hourly mean sustained wind speeds revealed that 991 h (78.9% of all freezing rain observations) had wind speed $< 10\,\mathrm{kt}$ ($1\,\mathrm{kt} = 0.51\,\mathrm{m\,s^{-1}}$), and about 46% of the mean 60-min wind speeds were between 5 and 10 kt. Figure 11 shows that there is a very gradual increase in ILR as the wind speed increases, particularly when analyzing the mean and 75th percentiles at values $> 9\,\mathrm{kt}$. ILRs increase the most at wind speeds $> 12\,\mathrm{kt}$, as seen by the increase in the mean and 75th percentile. Several of the highest ILRs in the dataset were associated with a wind speed $> 15\,\mathrm{kt}$, which accounted for <5% of all freezing rain observations. Another notable trend was a gradual increase in the 90th percentile values with increasing wind speed, lending support to previous research (J96). It is inferred that the increasing wind speed replaces air near the ice surface warmed by latent heat release, alters the droplet collision efficiency, increases the horizontal mass flux, and promotes evaporational cooling. Although, the data

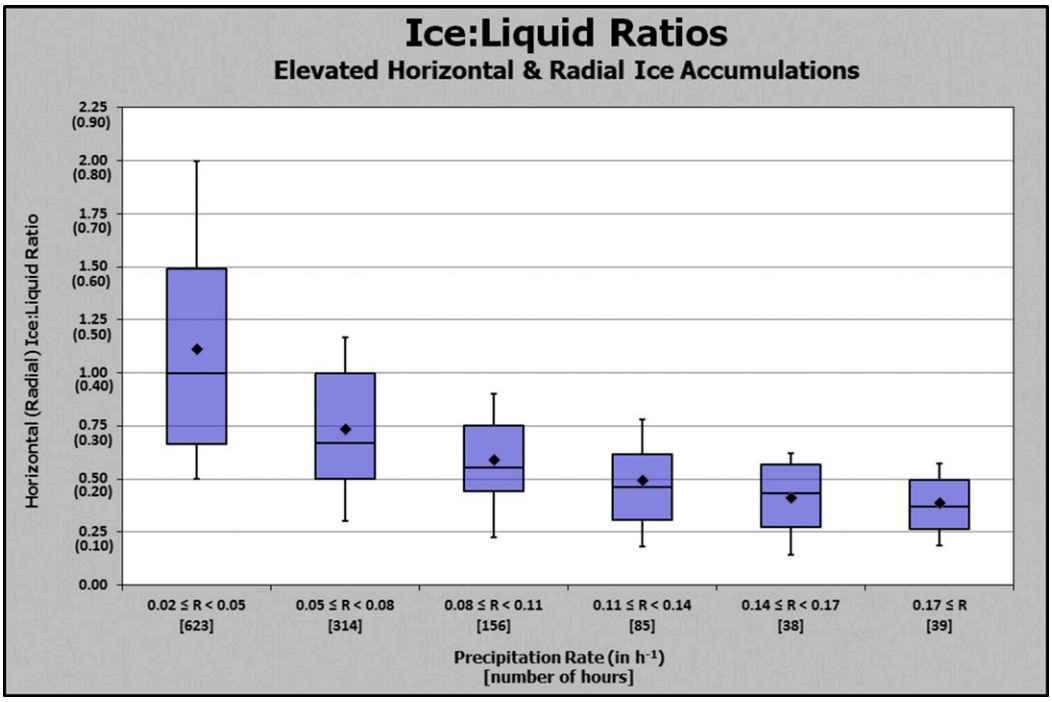

FIG. 10. As in Fig. 8, but for ILRs of elevated horizontal T_i and radial R_{eq} ice accumulations (purple) based on the precipitation rate (in. h^{-1}). The total numbers of hours are located below each range bin.

show that these processes are not as noticeable in the ILRs until wind speed reaches >15 kt, and may rely on the thermodynamic environment as well. Wind gusts had a similar influence on ILR with an increasing trend in ILR as wind gusts increased. However, the typical characteristic of a wind gust being infrequent over longer periods of time decreases its predictive ability in determining ice accretion efficiency. Increasing wind speed also enhances icing impacts once ice accretion has begun by putting stress on objects that have accumulated additional weight as a result of the ice load. In this way, increased wind speed and gusts can be responsible for additional damage to tree branches, power lines, and transmission towers during the freezing rain, and even well after it has ended.

d. Temperature and wet-bulb temperature

ILRs were calculated for both air temperature and wet-bulb temperature, and the analysis revealed these two variables showed similar trends with the exception of near-freezing conditions. While it may seem counterintuitive, there were 403 h (32.1% of all freezing rain observations) for which the mean 60-min temperature was ≥0°C. While some of this may be attributed to minor errors in ASOS temperature sensor calibration or icing surfaces that are colder than the ambient temperature, it was interesting to find that only 14 of these 403 h (1.1% of all freezing rain observations) had a mean 60-min wet-bulb temperature ≥ 0°C. The ILR also decreases substantially as the wet-bulb temperature approaches and exceeds 0°C, as seen in Fig. 12. These findings reveal that ice accretion is still possible at air temperatures > 0°C, but the icing is not as efficient as at colder temperatures. Ice accretion in these conditions may be highly dependent on the temperature of the icing surface, and also the magnitude of evaporational cooling, which is represented by the wet-bulb temperature. Statistical comparison of air temperature and wet-bulb temperature as a predictor of ILR (discussed in greater detail in section 4a) indicated that the coefficient of determination was greater for the wet-bulb temperature, and a *t* test comparing the mean error proved the wet-bulb temperature to have less error than air temperature at a greater than 98% confidence interval. This study has thus focused on using wet-bulb temperature as a predictive variable rather than air temperature. Relative humidity was also evaluated as a possible proxy for cooling due to evaporation, but had little to no effect as a single predictor for the ILR.

Figure 12 shows that the ILR tends to increase as the wet-bulb temperature decreases, and the greatest ILR occurs between −1° and −4°C with a median value near 0.80:1 within the given range. It is implied that lower wet-bulb temperatures lead to a greater efficiency in

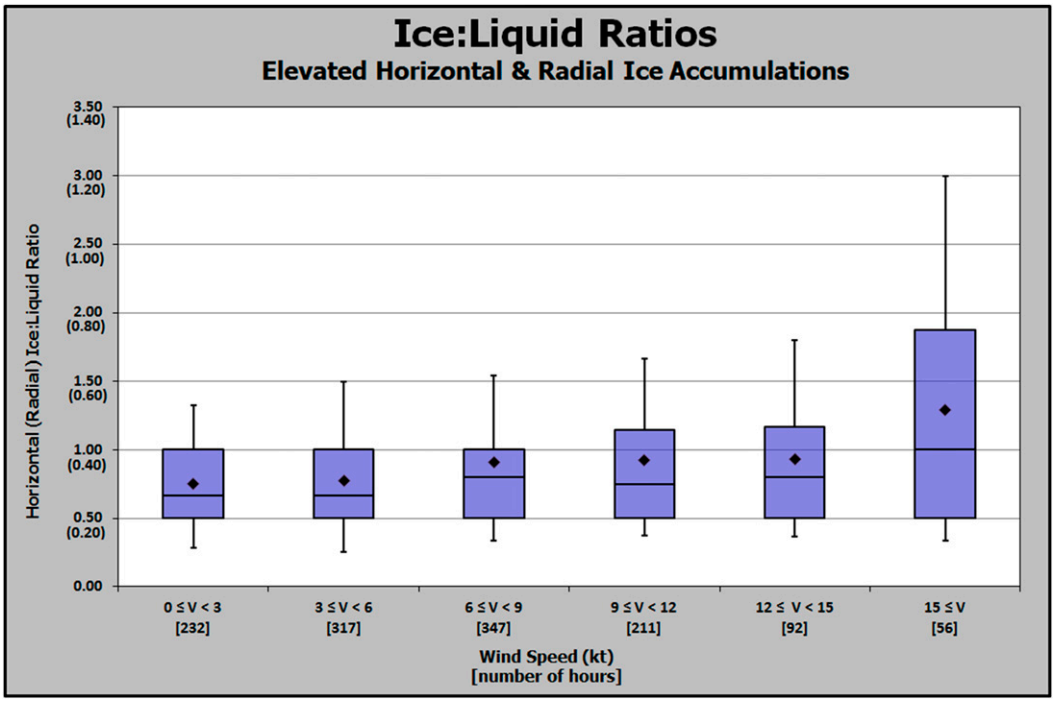

FIG. 11. As in Fig. 10, but based on hourly mean wind speed (kt).

freezing liquid as opposed to a near-freezing temperature, and these data illustrate that this resultant increase in ILR is most pronounced at wet-bulb temperatures lower than −1°C. One possibility is that more runoff is occurring with a near-freezing temperature, which may account for the lower ILR. Decreasing wet-bulb temperature will likely help offset the latent heat released, especially during increased wind speeds. Another

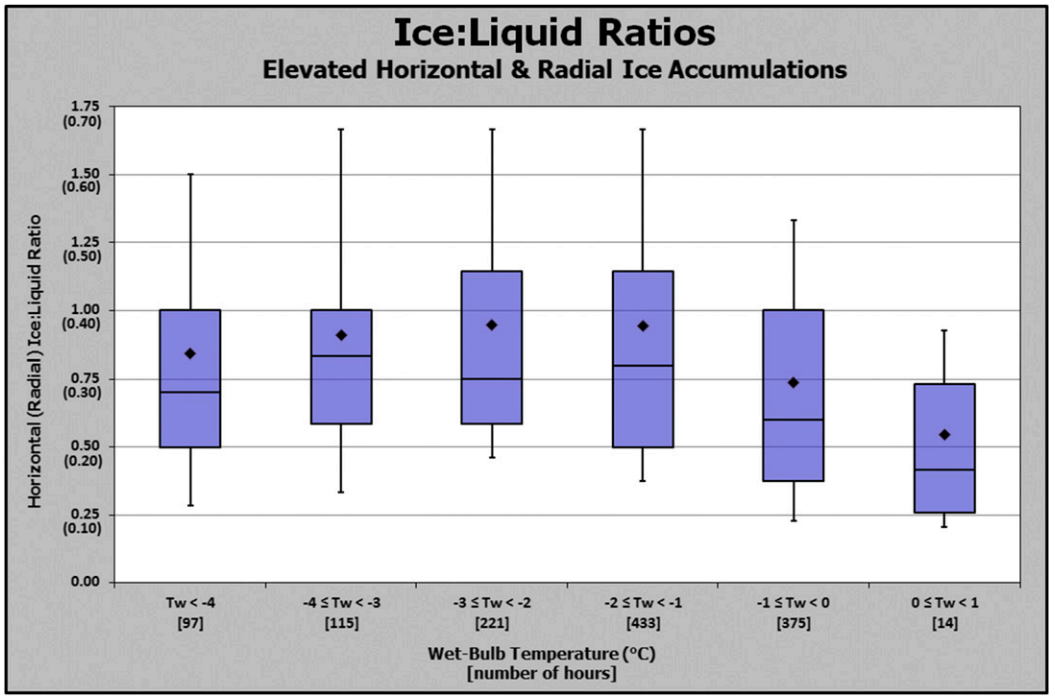

FIG. 12. As in Fig. 10, but based on hourly mean wet-bulb temperatures (°C).

temperature-related contributor to lower ILR may be due to liquid drops warming as they fall through an elevated warm layer, as it will require a greater negative heat flux from the water in order to freeze on contact. It has been hypothesized by some operational forecasters that during periods of near-freezing temperatures, high-precipitation rates can actually cause a rise in surface temperature through sensible heating of the drops that fall through an elevated warm layer and, perhaps, via downward advection of the warm-layer temperatures toward the surface.

Only 7.7% of all the freezing rain observations had a mean wet-bulb temperature < -4°C, with only 1% of the freezing rain observations occurring with a mean wet-bulb temperature < -6.5°C and none < -9°C. The data in this study indicate that despite the colder surface conditions, ILR actually decreases for wet-bulb temperatures < -4°C. Previous research by Stewart and Crawford (1995) as well as Zerr (1997) has shown there to be a greater likelihood of liquid drops refreezing into ice pellets (sleet) in near-surface cold layers that are at least 2.5 kft in depth and colder than −5°C. Rauber et al. (2001) found there is a correlation of −0.44 between the minimum temperature and depth associated with these near-surface cold layers, suggesting that it is possible to have a relatively shallow cold layer that is well below −5°C. In these situations it could be inferred that the liquid drop is not allowed enough time to refreeze before reaching the surface and instead remains freezing rain. Perhaps these lower temperatures lead to at least some mixture of ice pellets with the freezing rain, which is not identified by the ASOS present weather sensor. Even a small percentage of the precipitation falling as ice pellets would lead to a reduction of ILR, meaning a proportion of the precipitation produced in the cloud would be utilized for the production of both ice pellets and freezing rain. This effectively lowers the ratio of ice to total liquid precipitation. Regardless of the reason, the data consistently suggest that the ILR will decrease as the wet-bulb temperature decreases below −4°C. These results show the important effect that wet-bulb temperature plays in ice accretion efficiency, especially during near-freezing temperatures, and demonstrate the importance of utilizing wet-bulb temperature information in accurately forecasting ice accretion.

e. Comparison to CRREL SM

A further investigation into the CRREL SM reveals that precipitation rate and wind speed greatly influence ice prediction. While J98 demonstrated the CRREL SM's ability to create a quality forecast of ice load, there are some important assumptions made in these calculations. CRREL SM calculates radial ice thickness on an elevated cylindrical object (e.g., tree branches and power lines), and is not intended for use in forecasting ground-level icing or icing on horizontal surfaces, unless converted. CRREL SM assumes the air temperature to always be subfreezing, and that all water freezes immediately on contact. It ignores the effect of latent heat release, and also the possibility of water runoff to form into icicles or leave the surface all together. These assumptions could result in overforecasting ice accretion, particularly in near-freezing temperatures, light wind speeds, or with substantial dewpoint depressions (introducing the likelihood for evaporative cooling). The CRREL SM utilizes a droplet distribution adopted by Best (1950), which was used in calculating the liquid water content of the air during a typical rainfall. The Best (1950) distribution is more suited for larger drops (i.e., rain) and not smaller drops (i.e., drizzle), resulting in an underestimation of horizontal flux during small drop events. Another important assumption of the CRREL SM is that the cylindrical object ratio of length to diameter is very large, and that water spreads evenly over the entire surface. However, radial ice accumulation on a cylindrical object is independent of the diameter of the object, although an object with a larger (small) diameter has a larger (smaller) surface area, leading to a greater (lesser) mass of ice accumulated (J96). Finally, CRREL SM assumes the cylindrical object's long dimension is always perpendicular to the wind, which will maximize the horizontal mass flux. This makes sense in terms of forecasting a maximum possible ice load, but in a real-world scenario not every object will be perpendicular to the wind throughout the duration of an event.

Given its potential to be used in a forecast scenario, the CRREL SM forecasts were compared to the observed data. To examine the effects of precipitation rate and wind speed on the CRREL SM, each weather element (e.g., precipitation rate) was held constant while the other is adjusted (e.g., wind speed). Because of sample size issues, a range of precipitation rates and wind speeds were used to classify the ILR from the observed data as opposed to using one particular wind speed or precipitation rate. Since the CRREL SM forecasts radial ice thickness R_{eq}, the observed results were converted to R_{eq} using Eq. (1).

Precipitation rate has a much different effect on the CRREL SM results than on the observations, as seen in Fig. 13. The CRREL SM shows only minor change in ILR with increasing precipitation rates while the observed data show a much larger decrease in ILR with increasing precipitation rates. This can be accounted for by the CRREL SM using precipitation rate as a proxy for the liquid water content, resulting in a greater horizontal mass flux onto the surface as the precipitation rate increases. While the flux is indeed greater, this practice may lead to potentially invalid assumptions of

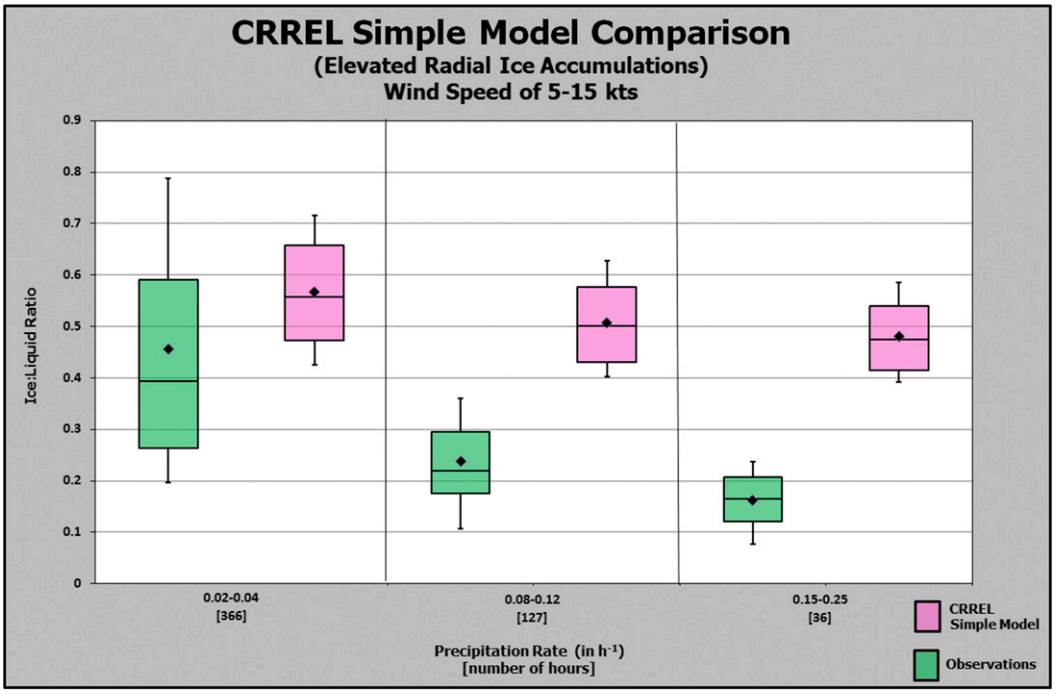

FIG. 13. A box-and-whisker comparison of ILRs from the CRREL SM (pink) to the observational data results (green) illustrating the effect of varying precipitation rates (in. h^{-1}) on ILRs. A wind speed range of 5–15 kt was held constant for each precipitation rate bin.

runoff and drop size distribution. Wind speed had a similar effect on the observed data as it does on the CRREL SM calculations, with ILR increasing with increasing wind speed. Figure 14 shows that the stronger wind speed causes a slightly greater increase in the predicted CRREL SM ILR than in the observed data. The observations also illustrate greater variability of ILR given uniform wind speed. Additional comparisons of ASOS icing data to CRREL SM and CRREL HBM can be found in Jones et al. (2004). In summary, the CRREL SM tends to overestimate ice accumulation in comparison to the observed data, and these overestimates are more pronounced with increasing precipitation rate, and to a lesser extent with increasing wind speed.

4. Freezing Rain Accumulation Model

a. Model development

One goal of this work was to improve the meteorological community's ability to predict freezing rain accumulation. In support of this, the analyses of individual weather elements and associated effects on ILR were further investigated and combined into a single predictive model. The Freezing Rain Accumulation Model (FRAM) predicts the hourly ILR based on three input variables of precipitation rate P, wind speed V, and wet-bulb temperature T_w. The ILR is then multiplied by the amount of liquid precipitation accumulation to predict the ice accumulation. The output of the FRAM will be an ice depth of T_i, but may be used to infer ice accretion on elevated cylindrical objects in terms of R_{eq} using Eq. (1). Given the 1-h temporal increments of the data, the FRAM is intended to also be used over 1-h predictive increments.

The initial step in the model creation was to analyze the data to maximize the skill of the predictor variables. We used various transformations on each predictor variable in relation to ILR to linearize the data. The preferred transformation model for each element was determined by the greatest coefficient of determination R^2. In the event that a polynomial regression equation produced the greatest R^2, forward selection stepwise regression was applied to ensure that the most significant terms were used. Finally, each individual equation had to be meteorologically reasonable. This final requirement for meteorological reasoning beyond the statistical analysis applied to the wet-bulb temperature polynomial regression equation. While the stepwise iteration suggested a quadratic equation provided significant results, a cubic regression better represented the sharp decline in ILR between 0° and 1°C given no freezing rain data points at $T_w > 1$°C. Even with the stepwise regression process suggesting the quadratic regression was sufficient, it should also be noted that there was a substantial

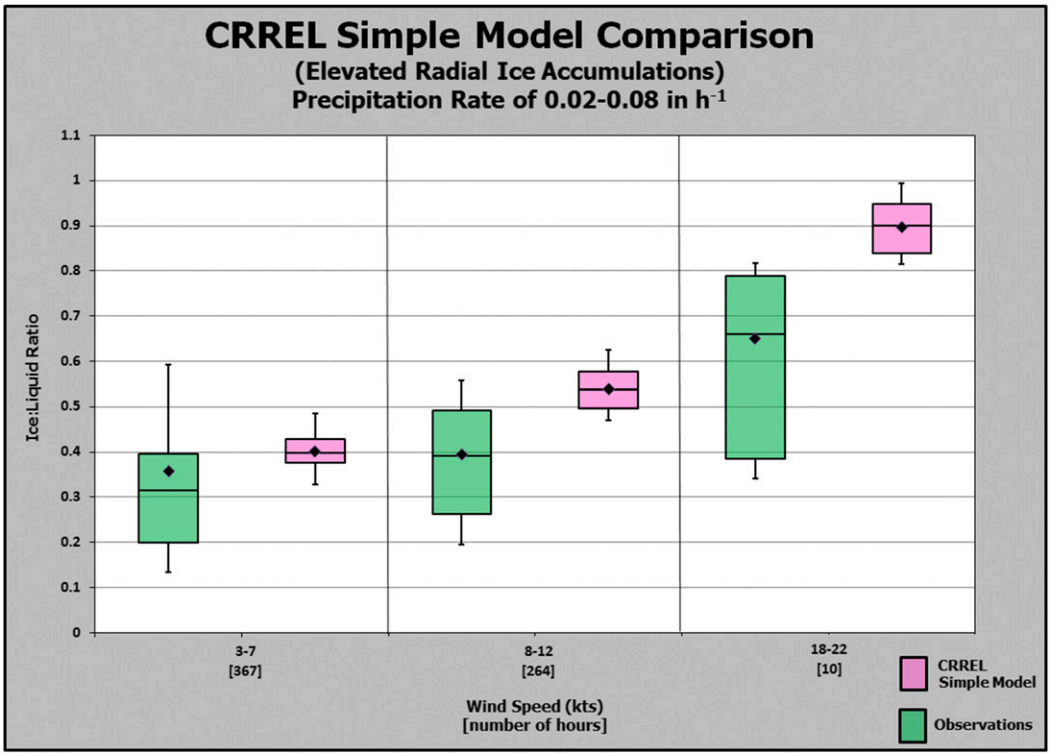

FIG. 14. As is Fig. 13, but illustrating the effect of varying wind speed (kt) on ILRs. A precipitation rate range of 0.02–0.08 in. h^{-1} was held constant for each wind speed bin.

improvement for R^2 in the transition to a cubic regression, with much smaller improvements for a quartic regression. Utilizing the cubic regression modeled a false increase in ILR at $T_w < -7$°C (<1% of total data points), which did not represent the observed data for these wet-bulb temperatures. For this reason, in the ILR calculation, all $T_w < -7$°C are set to $T_w = -7$°C. The regressions for each predictor variable can be seen graphically overlaid on the box-and-whisker diagrams in Fig. 15. The ILR regression equations for each predictor variable are defined here, where precipitation rate is indicated by P (in. h^{-1}), wet-bulb temperature by T_w (°C), and wind speed by V (kt):

$$\mathrm{ILR}_P(\text{precipitation rate}) = 0.1395(P)^{-0.541}, \quad (2)$$

$$\mathrm{ILR}_{T_w}(\text{wet-bulb temperature}) = -0.0071(T_w)^3 - 0.1039(T_w)^2 - 0.3904(T_w) + 0.5545, \quad \text{and} \quad (3)$$

$$\mathrm{ILR}_V(\text{wind speed}) = 0.0014(V)^2 + 0.0027(V) + 0.7574. \quad (4)$$

The next step in the model development was to optimally weight the predictive influence of each variable in the predictive process to maximize model forecast quality. An iterative analysis method using mean absolute error (MAE) as a deterministic measure of skill was used as the method for identifying the most effective weighting for each variable to maximize predictive ability. To identify the combination that produced the lowest MAE across the entire dataset, weighting of each individual regression equation was analyzed at 1% intervals and compared to every hour of the observational data until every possible weighting combination was analyzed. Additionally, anecdotal observations suggested that the impact of T_w and V may be of situationally varied importance, so regression weighting was further evaluated for improvement when using different weights with variations of T_w (iteratively analyzed at 0.05°C intervals) and V (iteratively analyzed at 1-kt intervals). While all three variables are important to ice accretion, this technique determined that there were situations for which the wet-bulb temperature had a greater effect on ILR than did the wind, and vice versa. This technique further reduced MAE by adjusting weighting functions of each regression equation situationally when the wet-bulb temperature is >-0.35°C or the wind speed is >12 kt.

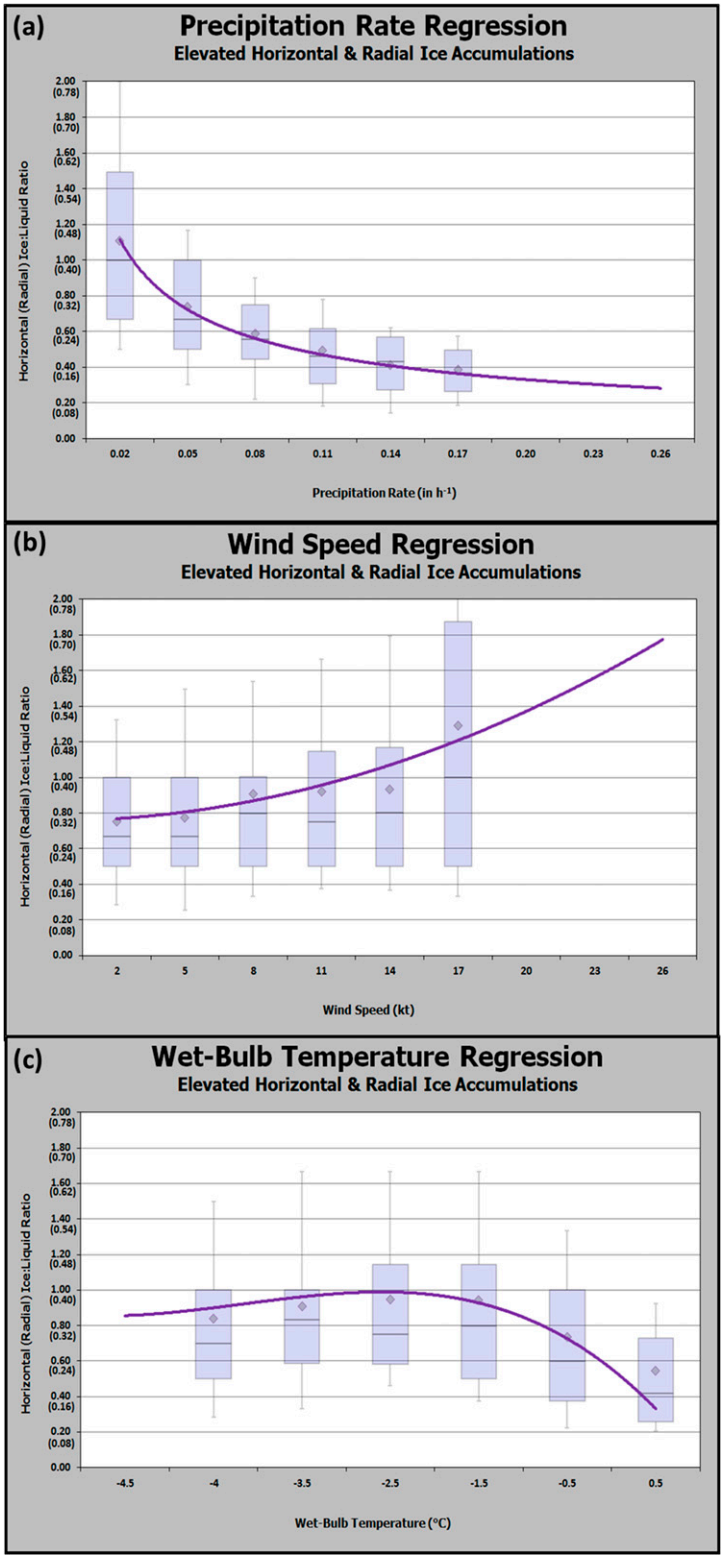

FIG. 15. Nonlinear regression trend lines of ILRs based on (a) precipitation rate (in. h^{-1}), (b) wind speed (kt), and (c) wet-bulb temperature (°C).

TABLE 1. Forecast model performance is shown for each of the 20 freezing rain events, selected randomly based on criteria defined in section 2. MAEs and total biases for the predictions of each forecast method are also displayed.

Case	ASOS site	City, state	Date	Duration (h)	Observed ice (in.)	Observed liquid precipitation (in.)	Observed ILR	FRAM forecast (in.)	FRAM error (in.)	CRREL SM forecast (in.)	CRREL SM error (in.)	1:1 ILR forecast (in.)	1:1 ILR error (in.)
1	AOO	Altoona, PA	26 Nov 2013	6	0.29	0.87	0.333	0.384	0.094	1.035	0.745	0.870	0.580
2	BIV	Holland, MI	21 Dec 2013	5	0.18	0.12	1.499	0.121	−0.059	0.241	0.061	0.120	−0.060
3	MTO	Matoon, IL	17 Feb 2014	3	0.13	0.18	0.722	0.129	−0.001	0.287	0.157	0.180	0.050
4	JLN	Joplin, MO	21 Dec 2013	11	0.34	0.55	0.618	0.411	0.071	0.775	0.435	0.550	0.210
5	DNL	Augusta, GA	12 Feb 2014	4	0.15	0.23	0.652	0.162	0.012	0.351	0.201	0.230	0.080
6	AUG	Augusta, ME	1 Dec 2013	3	0.08	0.10	0.801	0.084	0.004	0.156	0.076	0.100	0.020
7	LBT	Lumberton, NC	12 Feb 2014	6	0.24	0.51	0.471	0.340	0.100	0.739	0.499	0.510	0.270
8	VAY	Mount Holly, NJ	14 Dec 2013	3	0.16	0.23	0.695	0.140	−0.020	0.301	0.141	0.230	0.070
9	MEH	Meacham, OR	24 Feb 2014	3	0.05	0.09	0.556	0.085	0.035	0.105	0.055	0.090	0.040
10	MHE	Mitchell, SD	15 Dec 2014	4	0.17	0.22	0.773	0.151	−0.019	0.382	0.212	0.220	0.050
11	IND	Indianapolis, IN	11 Jan 2015	3	0.16	0.16	0.999	0.116	−0.044	0.237	0.077	0.160	0.000
12	PSF	Pittsfield, MA	4 Jan 2015	3	0.14	0.09	1.554	0.082	−0.058	0.140	0.000	0.090	−0.050
13	MSS	Massena, NY	4 Jan 2015	9	0.57	0.64	0.891	0.401	−0.169	0.876	0.306	0.640	0.070
14	FIG	Clearfield, PA	2 Feb 2015	4	0.16	0.23	0.695	0.163	0.003	0.309	0.149	0.230	0.070
15	THV	York, PA	12 Jan 2015	4	0.08	0.11	0.727	0.103	0.023	0.150	0.070	0.110	0.030
16	HGR	Hagerstown, MD	9 Dec 2014	6	0.43	0.58	0.742	0.332	−0.098	0.763	0.333	0.580	0.150
17	FWN	Sussex, NJ	9 Dec 2014	3	0.15	0.33	0.455	0.171	0.021	0.419	0.269	0.330	0.180
18	INK	Wink, TX	2 Jan 2015	6	0.24	0.54	0.444	0.319	0.079	0.676	0.436	0.540	0.300
19	FSM	Fort Smith, AR	28 Feb 2015	5	0.15	0.18	0.833	0.153	0.003	0.276	0.126	0.180	0.030
20	LWS	Lewiston, ID	4 Dec 2014	3	0.08	0.10	0.800	0.086	0.006	0.137	0.057	0.100	0.020
			Mean	4.7	0.20	0.30	0.76	MAE	0.046	MAE	0.220	MAE	0.116
								Bias	−0.001	Bias	0.220	Bias	0.106

The FRAM is defined as follows:
when $T_w > -0.35°\text{C}$,

$$\text{ILR} = (0.70\text{ILR}_P) + (0.29\text{ILR}_{T_w}) + (0.01\text{ILR}_V); \quad (5)$$

when $T_w \leq -0.35°\text{C}$ and $V > 12\,\text{kt}$,

$$\text{ILR} = (0.73\text{ILR}_P) + (0.01\text{ILR}_{T_w}) + (0.26\text{ILR}_V); \quad (6)$$

and
when $T_w \leq -0.35°\text{C}$ and $V \leq 12\,\text{kt}$,

$$\text{ILR} = (0.79\text{ILR}_P) + (0.20\text{ILR}_{T_w}) + (0.01\text{ILR}_V) \quad (7)$$

and

$$T_i = \sum_0^h \text{ILR} \times P. \quad (8)$$

The quantity T_i represents the final ice accumulation on an elevated horizontal surface, and Eq. (1) can be used to convert T_i to R_{eq} to best represent ice accumulation on tree branches and power lines. The h represents the number of hours over which the precipitation occurs.

For further detail regarding the robustness of the method, it should be noted that other statistical analysis methods were evaluated with less desirable results. An analysis of covariance was performed on the data with precipitation rate as a categorical variable, and the others as continuous variables. Additionally, because of the wide variation in precipitation rate, with a larger amount of data at lower values, a multiple linear regression was attempted using an equal number of data points across the precipitation range. While all of these methods did provide significant regressions, the results were nowhere near as accurate or predictive as was the FRAM.

b. *Model testing*

The NWS and meteorological community often rely on various methods or NWP models to predict ice accumulations. Two of these commonly used methods are a simple ILR (often 1.0:1) and the CRREL SM. These two forecast methods and FRAM were tested for their predictive ability using the control group of 20 randomly selected freezing rain events that had not been included in the FRAM development process. This control group of 20 icing events included a total of 94 h of freezing rain accumulation with observed total ice accumulations ranging from 1.27 to 14.48 mm (0.05 to 0.57 in.) per event. To remain consistent with the ASOS observations, all CRREL SM–predicted icing amounts were converted as needed to elevated horizontal ice accumulation T_i for direct comparison using the relationship discussed in

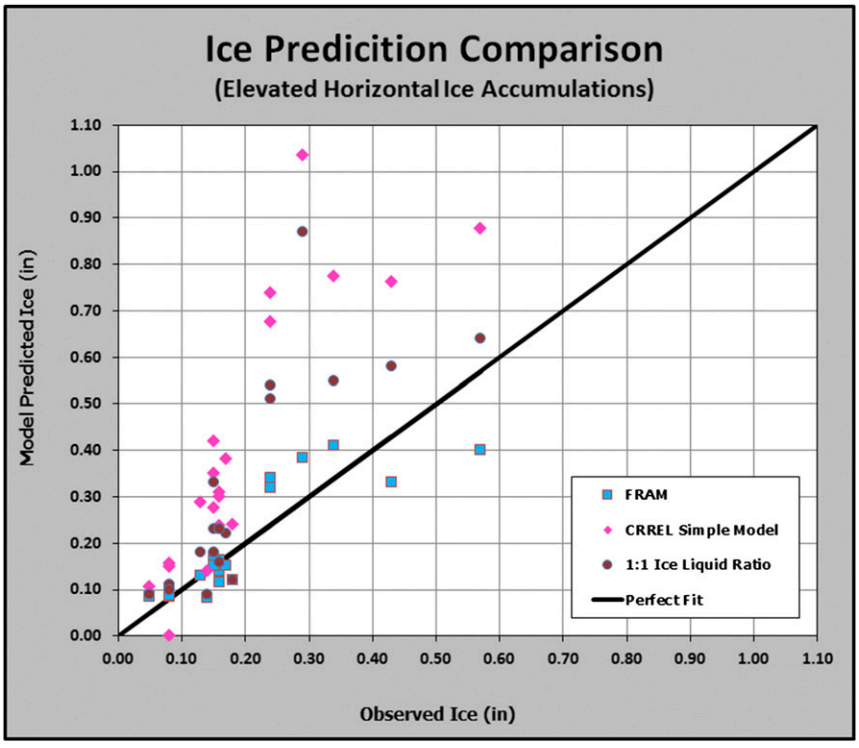

FIG. 16. Observed ice (in.) of the 20 randomly selected freezing rain events (total of 94 h) vs model-predicted ice (in.) from the FRAM (blue), CRREL SM (pink), and 1.0:1 ILRs (dark red). A perfect forecast is indicated by the heavy black line.

J98, which uses a factor of $1/\pi$ derived by simple geometry.

Examination of the total ice accumulation predictions from the FRAM for each of the 20 freezing rain events showed an MAE of 1.17 mm (0.046 in.) with a bias of −0.03 mm (−0.001 in.). The FRAM performed very well in comparison to the CRREL SM, which had an MAE of 5.59 mm (0.22 in.) and a bias of +5.41 mm (+0.213 in.), while the 1.0:1 ILR method had an MAE of 2.95 mm (0.116 in.) and a bias of +2.69 mm (+0.106 in.). The FRAM prediction of total ice accumulation was superior to both the CRREL SM and 1.0:1 ILR method for 17 of the 20 freezing rain events. Of the three events for which a non-FRAM forecast was superior, the most accurate forecast method only improved upon the FRAM forecast by a mean of 1.73 mm (0.068 in.). These results also further illustrate the tendency for the CRREL SM and 1.0:1 methods to overestimate the total icing amounts, particularly for events with greater precipitation rates. One-tailed paired-sample t tests showed that the FRAM MAE was less than both the CRREL SM MAE and the 1.0:1 MAE with greater than 99% confidence. The summary of results for all of the freezing rain events is presented in Table 1 while Figs. 16 and 17 directly compare the forecast error for the three techniques.

While FRAM performed very well over the test freezing rain events as a whole, it is important to understand any potential model limitations when using it in a forecast scenario. Regression equations for each individual element were developed in a deterministic fashion, and work together deterministically as well, but it is important to remember that all meteorological conditions are associated with a range of ILRs according to the observed data, and a range of results is possible, as evident in Fig. 15. It is important to note that FRAM output is dependent on any potential erroneous data input into the FRAM (e.g., NWP model with a P, T_w, or V bias or a poor NWP model forecast). Further attention may be needed when using FRAM during meteorological conditions that were sampled by less than 2% of the observation dataset. These include 1) wet-bulb temperature > 0°C, 2) wet-bulb temperature < -6°C, 3) wind speed > 20 kt, and 4) precipitation rate $> 6.35\,\text{mm}\,\text{h}^{-1}$ ($0.25\,\text{in.}\,\text{h}^{-1}$). Finally, FRAM was developed for freezing rain events with precipitation rates $\geq 0.50\,\text{mm}\,\text{h}^{-1}$ ($0.02\,\text{in.}\,\text{h}^{-1}$). Very light precipitation rates related to drizzle were not closely examined given the scope of this work.

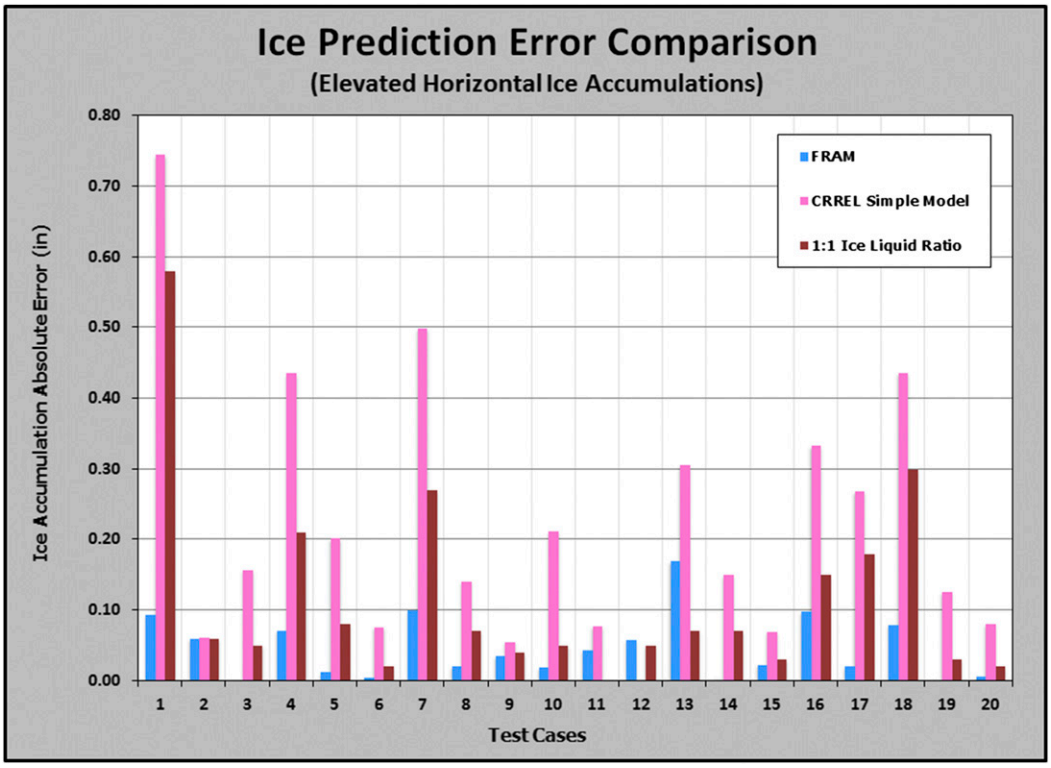

FIG. 17. Model-predicted ice accumulation absolute error (in.) for each of the 20 randomly selected freezing rain events from the FRAM (blue), CRREL SM (pink), and 1.0:1 ILRs (dark red). An absent bar indicates an error of zero.

5. Summary and conclusions

An analysis of 1255 ASOS 60-min icing, precipitation rate, wind speed, and wet-bulb temperature observations during freezing rain events revealed a relationship of these elements to ILR. The median ILR for all of the observations was 0.72:1, while the mean value was slightly higher at 0.87:1. Each of the aforementioned weather elements was investigated individually to identify the effects on the ice accretion process. Precipitation rate had the strongest correlation to ILR, and as the precipitation rate increases, ILR decreases. Wind speed also affects the ILR, particularly at speeds > 12 kt for which increasing wind speed results in a higher ILR. While temperature and wet-bulb temperature were both correlated to ILR, the wet-bulb temperature was found to have a stronger correlation and was particularly effective in near-freezing conditions > -1°C. The data showed that icing can commonly occur at air temperatures ≥ 0°C, particularly when the wet-bulb temperature is $\leq$0°C. The greatest icing efficiency occurred with wet-bulb temperatures between -1° and -4°C. Frequency of icing also followed a diurnal trend, with observations of freezing rain more frequent during the late evening and early morning and less frequent during the early afternoon.

A multivariable nonlinear regression Freezing Rain Accumulation Model (FRAM) was developed using the more than 1000 h of geographically diverse and objectively measured freezing rain data obtained for this study. FRAM was developed specifically with the intent of predicting ice accumulation through the use of commonly predicted meteorological variables, specifically precipitation rate, wind speed, and wet-bulb temperature. FRAM performance was tested against two other commonly used forecast methods, the CRREL SM and a 1.0:1 ILR, on 20 randomly selected freezing rain events with total icing ranging from 1.27 to 14.48 mm (0.05 to 0.57 in.). The FRAM was the most accurate forecast method for 17 of the 20 freezing rain events, with a total MAE of 1.17 mm (0.046 in.) and a bias of -0.03 mm (-0.001 in.). In comparison, the CRREL SM had an MAE of 5.59 mm (0.22 in.) and the 1.0:1 ILR method had an MAE of 2.95 mm (0.116 in.). One-tailed paired-sample t tests showed that the FRAM MAE was less than both the CRREL SM MAE and 1.0:1 MAE with greater than

99% confidence. The results of FRAM testing are encouraging and indicate that use of FRAM may be a notable step forward in improving ice accumulation forecasts for freezing rain events. Immediate future plans related to this work include collaboration testing during NWS operations and further investigation of ILR and accumulation characteristics during mixed precipitation and freezing drizzle events. Additional work is planned around the analysis of impacts resulting from damage, and the relation to ASOS ice accumulation amounts, which may be used to convey the severity of an icing event.

Acknowledgments. The authors express their sincere appreciation to the National Weather Service office in Topeka, Kansas, for their cooperation and support when conducting this research on site. We would also like to thank Darrel Smith for assisting with data collection, Brian O'Neill for assistance with the statistical evaluation, Dennis Cavanaugh for reviewing the methodology and statistics, and Dan Baumgardt and Phil Schumacher for offering their insight and input on this project. A special thanks to Scott Blair, Jason Schaumann, George Phillips, and Jeffrey Manion for their helpful reviews and technical editing.

REFERENCES

Ackley, S. F., and M. Templeton, 1979: Computer modeling of atmospheric ice accretion. CRREL Rep. 79-4, Cold Regions Research and Engineering Laboratory, Hanover, NH, 36 pp.

ASCE, 2002: *Minimum Design Loads for Buildings and Other Structures*. 2nd. ed. ASCE 7-02, American Society of Civil Engineers, Reston, VA, 376 pp.

Best, A. C., 1950: The size distribution of raindrops. *Quart. J. Roy. Meteor. Soc.*, **76**, 16–36, doi:10.1002/qj.49707632704.

Branick, M. L., 1997: A climatology of significant winter-type weather events in the contiguous United States, 1982–94. *Wea. Forecasting*, **12**, 193–207, doi:10.1175/1520-0434(1997)012<0193:ACOSWT>2.0.CO;2.

Chaîné, P. M., and G. Castonguay, 1974: New approach to radial ice thickness concept applied to bundle-like conductors. Industrial Meteorology Study, Vol. 4, AES Environment Canada, Toronto, ON, Canada, 22 pp.

Changnon, S. A., and T. G. Creech, 2003: Sources of data on freezing rain and resulting damages. *J. Appl. Meteor.*, **42**, 1514–1518, doi:10.1175/1520-0450(2003)042<1514:SODOFR>2.0.CO;2.

DeGaetano, A. T., B. N. Belcher, and P. L. Spier, 2008: Short-term ice accretion forecasts for electric utilities using the Weather Research and Forecasting Model and a modified precipitation-type algorithm. *Wea. Forecasting*, **23**, 838–853, doi:10.1175/2008WAF2006106.1.

Hosking, J. R. M., and J. R. Wallis, 1987: Parameter and quantile estimation for the generalized Pareto distribution. *Technometrics*, **29**, 339–349, doi:10.1080/00401706.1987.10488243.

Jones, K. F., 1996: Ice accretion in freezing rain. CRREL Rep. 96-2, Cold Regions Research and Engineering Laboratory, Hanover, NH, 23 pp. [Available online at www.dtic.mil/cgi-bin/GetTRDoc?AD=ADA310659.]

——, 1998: A simple model for freezing rain ice loads. *Atmos. Res.*, **46**, 87–97, doi:10.1016/S0169-8095(97)00053-7.

——, A. C. Ramsay, and J. N. Lott, 2004: Icing severity in the December 2002 freezing rain storm from ASOS data. *Mon. Wea. Rev.*, **132**, 1630–1644, doi:10.1175/1520-0493(2004)132<1630:ISITDF>2.0.CO;2.

Makkonen, L., 1984: *Atmospheric Icing on Sea Structures. CRREL Monogr.*, No. 84-2, Cold Regions Research and Engineering Laboratory, Hanover, NH, 92 pp. [Available online at http://www.bsee.gov/Technology-and-Research/Technology-Assessment-Programs/Reports/001-099/056AC/.]

——, 1998: Modeling power line icing in freezing precipitation. *Atmos. Res.*, **46**, 131–142, doi:10.1016/S0169-8095(97)00056-2.

Musilek, P., D. Arnold, and E. P. Lozowski, 2010: An ice accretion forecasting system (IAFS) for power transmission lines using numerical weather prediction. *SOLA*, **5**, 25–28, doi:10.2151/sola.2009-007.

NWS, 1995: Freezing precipitation algorithm. Automated Surface Observing System Contract 50-SANW-0050, Appendix I, Section 6.3.1.1, C-A-I-6-9.

——, 2000: Add ice accretion remark to METAR/SPECI reports. NWS Engineering Change Proposal S01126, NWS/OM22 and NWS/OSO1 × 4, 45 pp.

Ramsay, A. C., and M. E. Laster, 1995: Status of the ASOS freezing rain sensor. Preprints, *Sixth Conf. on Aviation Weather Systems*, Dallas, TX, Amer. Meteor. Soc., 460–465.

Rauber, R. M., L. S. Olthoff, M. K. Ramamurthy, D. Miller, and K. E. Kunkel, 2001: A synoptic weather pattern and sounding-based climatology of freezing precipitation in the United States east of the Rocky Mountains. *J. Appl. Meteor.*, **40**, 1724–1747, doi:10.1175/1520-0450(2001)040<1724:ASWPAS>2.0.CO;2.

Ryerson, C. C., and A. C. Ramsay, 2007: Quantitative ice accretion information from the automated surface observing system. *J. Appl. Meteor.*, **46**, 1423–1437, doi:10.1175/JAM2535.1.

Sanders, K. J., C. M. Gravelle, J. P. Gagan, and C. E. Graves, 2013: Characteristics of major ice storms in the central United States. *J. Oper. Meteor.*, **1** (10), 100–113, doi:10.15191/nwajom.2013.0110.

Stewart, R. E., and R. W. Crawford, 1995: Some characteristics of the precipitation formed within winter storms over eastern Newfoundland. *Atmos. Res.*, **36**, 17–37, doi:10.1016/0169-8095(94)00004-W.

Zerr, R. J., 1997: Freezing rain: An operational and theoretical study. *J. Appl. Meteor.*, **36**, 1647–1661, doi:10.1175/1520-0450(1997)036<1647:FRAOAT>2.0.CO;2.